Observation of Quantum-Size Effects at Room Temperature on Metal Surfaces With STM

Phaedon Avouris and In-Whan Lyo

Surface steps act as confining barriers for electrons in metal-surface states. Thus, narrow terraces and small single-atom–high metal islands act as low-dimensional, electron-confining structures. In sufficiently small structures, quantum-size effects are observable even at room temperature. Scanning tunneling spectroscopy is used to image the probability amplitude distributions and discrete spectra of the confined states. Examination of the electronic structure of the steps provides evidence for electron-density smoothing and the formation of step-edge states. Estimates of the electron-confining barriers are obtained.

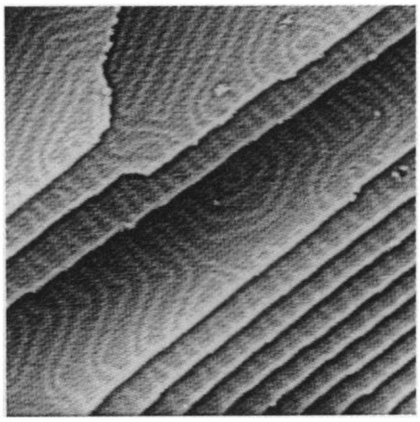

Fig. 1. Constant-current STM image of a stepped Au(111) surface. The sample bias is +0.23 V. The pairs of lines seen on the terraces are due to the $22x\sqrt{3}$ reconstruction of the Au(111) surface.

The study of the physics of electrons in low-dimensionality structures has been an active area of research, the results of which have an important impact on both basic science and technology (*1*). Two types of two-dimensional (2D) electron systems have received wide attention: (i) electrons trapped at the surface of liquid He and (ii) electrons trapped in inversion layers at the metal-insulator interfaces or electrons at semiconductor heterojunctions (*1*). Confinement and further decreases in dimensionality are usually achieved by patterning of the 2D electron gas layer by lithography or by electric field–induced confinement. Here, we discuss a different type of 2D electron system involving electrons in metal-surface states, the study of which has become accessible thanks to recent developments in scanning tunneling microscopy (STM). We will show that very small (a few nanometers), low-dimensional structures can be formed naturally at metal surfaces and that they exhibit quantum-size effects observable even at room temperature. The study of such electronic effects may lead to new insights on surface processes such as diffusion, film growth, and surface chemistry.

At certain faces of metals, such as the (111) faces of noble metals, the surface electrons are confined to the vicinity of the top layer by the vacuum barrier on one side and a band gap in the bulk states on the other side (*2*). The electrons in these Shockley-type surface states (*2*) behave like a high-density 2D electron gas (*3*). Recently, it was shown that STM and scanning tunneling spectroscopy (STS) can be used to study the interactions of this electron gas with localized surface scatterers such as surface steps and adsorbates (*4–6*). Electrons incident on a step are partially reflected, and the interference between incident and reflected waves leads to an oscillatory local density of states (LDOS) that can be imaged in STM topographs or STS maps (*5, 6*). The analysis of such STM experiments provides information on both the surface state and the scattering process. Here, we show that natural boundaries, such as surface steps, can be used to generate stable confined-electron structures with sizes much smaller than the size of analogous structures produced by conventional lithography. A different approach involving the arrangement of adsorbed atoms with the scanning tunneling microscope to form structures (corrals) that are stable at low temperatures and that can confine electrons has also been demonstrated recently (*7*).

The experimental STM and STS setups used in this study have been described elsewhere (*8*). Similarly, experimental information on sample preparation can be found in (*9*). A natural way of forming low-dimensional structures at metal surfaces includes the controlled growth of epitaxial layers. By the appropriate choice of deposition and annealing temperatures, stepped surfaces with narrow terraces or islands with variable size and shape can be generated (*10*). Control over the terrace width can be achieved easily by the use of vicinal surfaces (*11*), which are prepared by the cutting of a single crystal surface at a small angle with respect to a low-index crystal plane. In Fig. 1, we show a stepped Au(111) surface produced by controlled epitaxy on a mica substrate (*9*). The parallel lines seen on the terraces arise from the well-known $22x\sqrt{3}$ herringbone reconstruction of Au(111) (*12*). The width of the narrow terraces in Fig. 1 is about 8 nm; narrower and wider widths can easily be obtained. If we denote the direction normal to the steps as x and the direction parallel to the steps as y, we expect that the surface electrons on each terrace would be confined by the steps in the x direction but would be free in the y direction. Thus, the wave functions of surface electrons in the x direction would be standing waves, while in the y direction they would be plane (Bloch) waves. The standing wave patterns would be similar to the probability amplitude distribution of the states of a particle in a 1D potential-energy well. However, in a proper analysis of the problem it is essential to include the effects of the continuum of the plane-wave states in the y direction.

To investigate the electronic structure of the system, we have obtained, simultaneously with the constant-current STM topographs, tunneling current-voltage (I-V) curves. Specifically, at intervals of ~2 Å, the STM scanning is interrupted and the feedback loop is deactivated. Then, with the position of the tip fixed, the tunneling current is measured as a function of the voltage applied to the sample. The resulting I-V curves are used to obtain the differential conductance dI/dV, which is roughly proportional to the LDOS (*13*). In this way, dI/dV line scans perpendicular to the step are generated. These line scans are laterally averaged to increase the signal-to-noise ratio. Results for a 36 Å–wide gold terrace are shown in Fig. 2. A 3D map of dI/dV (~LDOS) as a function of the distance perpendicular to the steps and of the applied bias (energy) is given in Fig. 2A, while individual dI/dV line scans are shown in Fig. 2B for different values of the voltage applied to the sample. The voltage varies from −0.47 V (bottom) to +0.39 V (top). The stabilization voltage of the constant-current scan is V_s = +0.23 V. The first line scan (bottom of Fig. 2B) is taken at an energy just below the onset of the surface state that is placed at −0.41 eV below the Fermi level (E_F) (*14*). The 3D map and the line scans show two peaks (denoted by S) centered at the lower edges of the two steps traced by the STM topographic scan (dotted line). The intensity of these peaks is seen to vary with the applied bias. These peaks may signify the presence of a 1D "step-edge" state. Such states can be produced as a result of the reduced coordination of the step atoms (*15*). At about

---

IBM Research Division, T. J. Watson Research Center, P.O. Box 218, Yorktown Heights, NY 10598, USA.

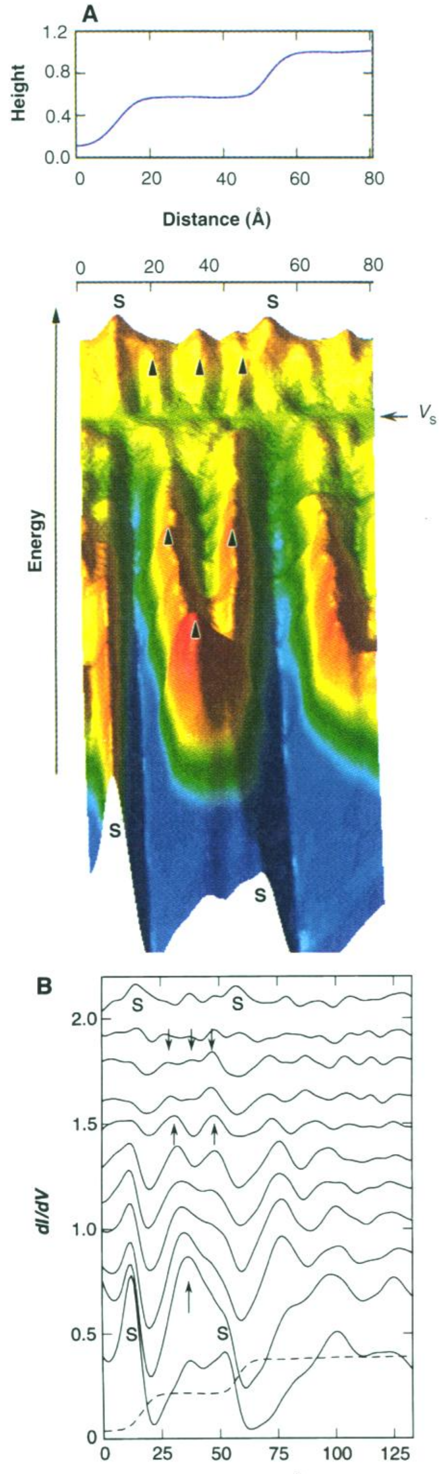

Fig. 2. Probability amplitude distribution of the confined electron states of a 36 Å Au(111) terrace. (**A**) A 3D map of *dI/dV* ($\sim$LDOS) as a function of the distance perpendicular to the steps and of the voltage applied to the sample (energy). The bias ranges from -0.47 V (bottom) to $+0.38$ V (top). The height values are given in arbitrary units. (**B**) Individual *dI/dV* line scans for different sample voltages. Values for *dI/dV* are given in arbitrary units. The stabilization voltage V_s was $+0.23$ V. The dotted line is a constant-current STM line scan, and step-edge peaks are marked by S.

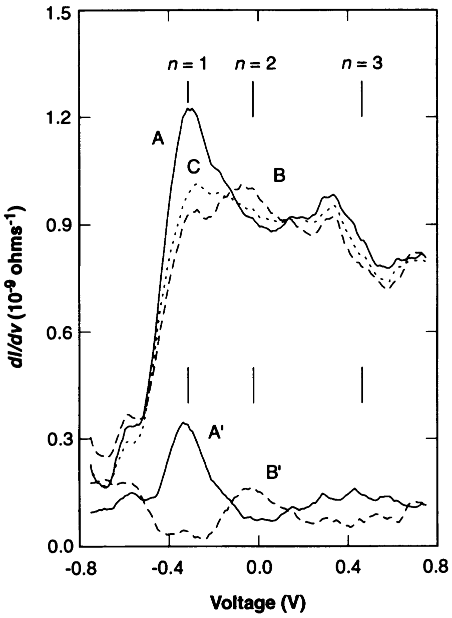

Fig. 3. Spectra for *dI/dV* of the confined states of a 36 Å–wide terrace at room temperature. Curve A was obtained at the middle of the terrace, curve B was obtained at a distance of about one-quarter of the terrace width from the step, and curve C was over a wide (not confined) terrace.

-0.33 V (or at $\sim$80 meV above the onset of surface state), the LDOS shows a single peak situated at the middle of the narrow terrace. This peak corresponds to the probability amplitude distribution, $|\Psi|^2$, of the $n = 1$ confined state in the x direction. As the voltage is increased, we observe a gradual evolution to a two-peak pattern. At a voltage of about -0.01 V, a symmetric two-peak structure is observed. This structure corresponds to the amplitude distribution of the $n = 2$ confined state. Finally, at about $+0.41$ V, a three-peak pattern characteristic of the $n = 3$ state is observed.

A different way to study the confined states involves the measurement of the spectra, *dI/dV* versus the voltage, at specific locations on the crystal terrace. For example, for a symmetric potential well, spectra obtained at the center of the terrace would only show peaks corresponding to odd quantum states, because even states should have a node at that position. Figure 3 shows a number of such spectra. Curve A obtained at the center of the narrow terrace shows a peak at $\sim$0.33 V below E_F, corresponding to the $n = 1$ state. Additional structure is seen, but this structure does not depend on the position on the surface and could be tip-related (several different W tips showed this structure). Curve B is obtained at a point situated about one-quarter of the terrace width from the step. It shows a peak at $\sim$0.29 eV above the $n = 1$ state, in agreement with the expectations for the confined $n = 2$ state. A small peak is also seen at the energy of the $n = 1$ state, as is expected from an inspection of Fig. 2. Curve C is obtained on the upper, wide terrace at a point sufficiently far removed from any steps. It shows the onset of the surface state, but no peaks at the positions of the $n = 1$ and $n = 2$ confined states. Curve A′ gives the difference between curve A and curve C and shows not only the $n = 1$ state peak but also a broad peak centered at $\sim$0.43 eV that corresponds to the $n = 3$ state. Curve B′ gives the difference between curve B and curve C and shows the $n = 2$ peak.

Several effects contribute to the width of the observed spectra: lifetime broadening, thermal broadening, and the continuum of the electron states in the unconfined y direction. The last provides the dominant contribution to the broadening of the spectral peaks. By an increase in the bias voltage, the energy of the surface electrons, and therefore the wave number, $k_{\parallel}$, in the plane of the surface is increased. Resonances (confined states) appear at specific values of k_x. Because $k_x = \sqrt{k_{\parallel}^2 - k_y^2}$, a continuous spectrum should be produced. However, the probability density of k_y in one dimension is a decreasing function of the energy

$$P(k_y) \sim (E_0 - E)^{-1/2}$$

where E_0 is the energy onset of the confined state. Thus, a broadened but discrete spectrum results.

The results shown in Figs. 2 and 3 clearly demonstrate the ability both to image the probability amplitudes and to obtain the spectra of confined states at metal surfaces even at room temperature. We have attempted to obtain additional information on the confinement produced by surface steps by comparing the experimental results with the predictions of a simple model. In our previous STM studies of electron scattering by surface steps (5), we concluded that the reflection of electrons incident at a step from the side of the upper terrace is stronger than the reflection of electrons incident on the step from the lower terrace side. For certain step orientations, the barrier on the upper side of a step was found to be well represented by a hard-wall potential (5, 6). It is likely that electrons incident at the lower side of the step can more easily be transmitted into empty bulk states. Surface and bulk states are orthogonal; however, the presence of the step allows bulk-surface mixing. Thus, in our simple model of a terrace of width a, we place a hard-wall barrier at the upper side of the step leading to the lower terrace, which we take as the origin. That is, at $x = 0$, $V_U = \infty$, and at $x = a$ (at the bottom of the step leading to the upper terrace), we place a delta function barrier so that $V_L =$

$V_0\delta(x - a)$, where V_0 is variable. An approximate value of V_0 is obtained by comparison of the relative intensities of interference oscillations produced by scattering from the upper and lower sides of a step at wide terraces and by simulations of the line scans (Fig. 2) and spectra (Fig. 3). The wave function of the electrons in the narrow terrace was taken to be of the form

$$\Psi(k_\parallel) = A \sin k_x x \exp(ik_y y)$$

and the 2D and 1D local density of states was calculated.

The simulations based on the above model reproduce well the *dI/dV* line scans of Fig. 2. The simulations of the line scans, of the spectra, and of the relative oscillation amplitudes indicate that the effective V_L barrier is low, characterized by a value for V_0 of 1 ± 0.5 eV·Å. In Fig. 4, we show calculated spectra for the STM tip positioned at the middle of the 36 Å–wide terrace. For large values of V_0, only the odd ($n = 1, 3$) states are observed at the center of the step and the spectral width (at $T = 0$ K) is small. As V_0 is decreased, the width of the spectral lines increases. At the same time, the asymmetry of the two types of steps increases and the even ($n = 2$) state now appears weakly as a shoulder, as in the case of the experimental spectra (Fig. 3). The relative importance of the broadening due to a finite step barrier and that due to the unconfined motion in the y direction can be obtained by comparison of the 2D and 1D density of states for the same value of V_0. Thus, for $V_0 = 1$ eV·Å, the full width at half maximum of the $n = 1$ state at $T = 0$ K is found to be 20 meV (1D) and 80 meV (2D). Another manifestation of the interaction in two dimensions is the observed asymmetry of the spectral lines, which is present only when two dimensions are included and persists even after thermal broadening is introduced. The low intensity of the $n = 3$ peak is due to the fact that its energy lies close to the stabilization bias used in the experiment. Studies of wider terraces, but with widths comparable to the coherence length at room temperature, allow the observation of a larger number of confined levels. We have observed confined states in terraces with widths in the range of 30 to 60 Å. The energies of the confined states were found to scale as $\sim(\text{width})^{-2}$.

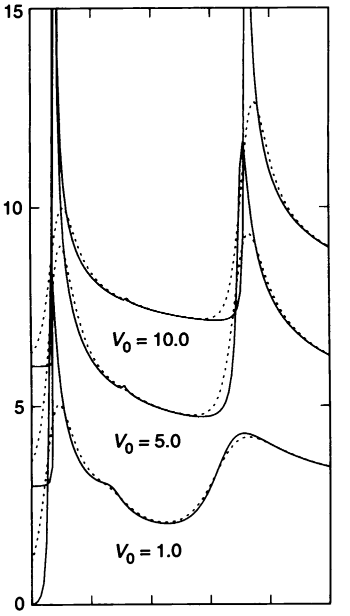

Fig. 4. Simulation of the spectra of the confined states of a 36 Å–wide terrace as a function of the confining barrier V_0. Values for *dI/dV* are given in arbitrary units. At the middle of the terrace, $m^* = 0.28$. Solid trace, $T = 0$ K; dotted trace, $T = 300$ K.

We now briefly return to discuss the origin of the step-edge peaks. In a previous study [Avouris and colleagues (*5*)], we showed that the Au(111) surface-state spectrum is not observed when the tip is over a step. This observation agrees with the fact that the step-edge peaks (S) in Fig. 2 are observed at energies below the onset of the surface state. While these peaks are localized to the vicinity of the steps, they are observed to change their position as the sign of the applied bias is changed, that is, as the energy is swept through the Fermi level. Specifically, the peaks are centered near the bottom of the step when the sample bias is negative, so that occupied states are probed (see bottom of Fig. 2B). The peaks move 3 to 4 Å toward the top of the step when the bias is positive and unoccupied states are probed (see top of Fig. 2B). These changes provide a clue for the origin of the peaks. In considering the electronic structure at a metal step, Smoluchowski (*16*) pointed out that for the electron kinetic energy, which is proportional to the square of the gradient of the wave function, to be minimized at step edges, there would be a "smoothing effect," where the electron density will not follow the abrupt change in geometry but will flow from the upper step edge into the lower step wedge. As a result of this electron-density smoothing, there is a local increase of the electron density at the bottom of the step and a corresponding decrease at the top. The observed movement of the edge peaks may reflect the above changes in electron density. The charge rearrangement generates a step dipole with an orientation opposite that of the surface electronic dipole present in flat areas of the surface. This effect is responsible for the lower work function of stepped surfaces (*17*); it would lead to a reduced effective barrier and enhance tunneling near the step, giving rise to the step-edge peaks.

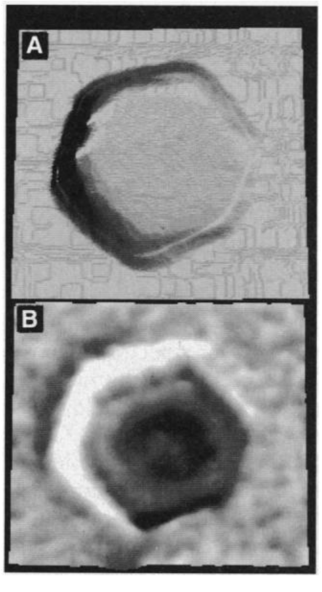

Fig. 5. (**A**) STM topograph of a 45 Å–wide Ag island. (**B**) A *dI/dV* image of the same island at a sample bias of −0.01 V.

Finally, we consider briefly the case of electron confinement at metal islands. The quantum structures generated in this way can be at least an order of magnitude smaller than structures fabricated with lithographic techniques. In Fig. 5 we show an Ag(111) island that is a single atom high with a "radius" of ~45 Å grown on a polycrystalline Ag substrate. In Fig. 5A we show an STM image of this hexagonal island and in Fig. 5B we show a *dI/dV* image obtained at an energy of ~110 meV above the onset of the Ag(111) surface state. While the STM image shows structure on the surface of the island, the *dI/dV* image shows a clear standing wave pattern encompassing the island. From the previous discussion, we expect the confining potential barriers to be high, because only upper sides of steps are involved in the confinement of the electrons. For simplicity, we can approximate the states of the hexagonal island with the states of a circular box (*18*). The energies will then be given by

$$E_{n,\ell} = E_0 + \hbar^2 u_{n,\ell}^2 (2m^* a^2)^{-1}$$

and the wave functions by

$$\Psi_{n,\ell}(r,\phi) \propto J_n(u_n r/a) \exp(i\ell\phi)$$

where $\hbar = h/2\pi$ (h = Planck's constant), a is the radius, n and ℓ are quantum numbers, ϕ is the azimuthal angle, J_n is the nth-order Bessel function, and $u_{n,\ell}$ is the ℓth root of this function. Considering the amplitude distributions of the circular-box states, we recognize that the nodal characteristics of Fig. 5B are those of the $n = 0$, $\ell = 2$ state. However, the central peak is much weaker than it should be, indicating the presence of a second state. With the above expression for the energy, we find that there are two states near 100 meV: the $n = 0$, $\ell = 2$ state (108 meV) and a doubly degenerate $n = 2$, $\ell = 1$ state (93 meV). These two states are not resolvable at room temperature by STS. A simulation of the image in Fig. 5B shows that it can be fitted by a superposition of two-state densities: about 80% of the (2, 1) and 20% of the (0, 2) state, in good agreement with the expectations from the simple circular-box model.

Concerning the use of metallic structures such as those studied here as models for the study of electron confinement, we note that in the simplicity of their generation and stability, such structures have advantages over corrals formed by atomic manipulation at liquid-helium temperatures (*7*). Atomic manipulation, however, can be implemented in conjunction with the natural structures. It can be used to modify these structures or dope them with specific atoms to, for example, model scattering during electrical transport processes. The charge-density distributions and field gradients resulting from confined states, such as in a growing interface, are different from those at an extended terrace. These factors are likely to influence surface processes that depend on them, such as the sticking, diffusion, and spatial distribution of adatoms and the growth of islands. The STS methods provide a powerful tool to start exploring these issues.

REFERENCES AND NOTES

1. L. Esaki, Ed., *Highlights in Condensed Matter Physics and Future Prospects*, vol. 285 of *NATO ASI Series* (Plenum, New York, 1991); T. Ando, A. B. Fowler, F. Stern, *Rev. Mod. Phys.* **54**, 437 (1984); M. A. Reed and W. P. Kirk, Eds., *Nanostructure Physics and Fabrication* (Academic Press, New York, 1989).
2. F. Forstmann, in *Photoemission and the Electronic Properties of Surfaces*, B. Feuerbacher, B. Fitton, R. F. Willis, Eds. (Wiley, New York, 1978), pp. 193–226; H. Luth, *Surfaces and Interfaces of Solids* (Springer-Verlag, Berlin, 1993).
3. N. W. Ashcroft and N. D. Mermin, *Solid State Physics* (Saunders, Philadelphia, 1976).
4. L. C. Davis, M. P. Everton, R. C. Jaklevic, W. Shen, *Phys. Rev. B* **43**, 3821 (1991).
5. Y. Hasegawa and Ph. Avouris, *Phys. Rev. Lett.* **71**, 1071 (1993); Ph. Avouris, I.-W. Lyo, R. E. Walkup, Y. Hasegawa, *J. Vac. Sci. Technol. B* **May, June** (1994).
6. M. F. Crommie, C. P. Lutz, D. M. Eigler, *Nature* **363**, 524 (1993).
7. ———, *Science* **262**, 218 (1993).
8. Ph. Avouris and R. Wolkow, *Phys. Rev. B* **39**, 5071 (1989).
9. Y. Hasegawa and Ph. Avouris, *Science* **258**, 1763 (1992).
10. H. Roder, E. Hahn, H. Brune, J.-P. Bucher, K. Kern, *Nature* **366**, 141 (1993).
11. G. A. Somorjai, *Chemistry in Two Dimensions: Surfaces* (Cornell Univ. Press, Ithaca, NY, 1981).
12. U. Harten, A. M. Lahee, J. P. Toennies, Ch. Woll, *Phys. Rev. Lett.* **54**, 2619 (1985).
13. A. Selloni, P. Carnevali, E. Tosatti, C. D. Chen, *Phys. Rev. B* **31**, 2602 (1985).
14. S. D. Kevan and R. H. Gaylord, *Phys. Rev. B* **36**, 5809 (1987).
15. H. Namba, N. Nakanishi, T. Yamaguchi, H. Kuroda, *Phys. Rev. Lett.* **71**, 4027 (1993).
16. R. Smoluchowski, *Phys. Rev.* **60**, 61 (1941).
17. K. Besocke and H. Wagner, *Surf. Sci.* **52**, 653 (1975).
18. J. R. Platt, *J. Chem. Phys.* **22**, 1448 (1954).

19. We thank R. E. Walkup for useful discussions.

28 January 1994; accepted 30 March 1994

Diacetylenic Lipid Tubules: Experimental Evidence for a Chiral Molecular Architecture

J. M. Schnur,* B. R. Ratna, J. V. Selinger, A. Singh, G. Jyothi, K. R. K. Easwaran

Molecular self-assembly is of key importance for the rational design of advanced materials. To investigate the causal relation between molecular structure and the consequent self-assembled microstructure, self-assembled tubules of diacetylenic lipids were studied. Circular-dichroism studies give experimental evidence that the formation of tubules is driven by chiral molecular packing, in agreement with recent theories of tubules. On the basis of these results, a molecular mechanism for the formation of tubules is proposed.

Molecular self-assembly has the potential to enable the fabrication of technologically useful microstructures, because it may be possible to "engineer" these micrometer-scale structures by "tweaking" the structure of their constituent molecules (*1*, *2*). To develop rational design rules for self-assembled materials, one must understand the causal relation between the molecular structure and the resulting microstructure. As a first step in understanding this relation, several research groups have studied the self-assembly of cylindrical tubules. Tubules are composed of membranes of amphiphilic molecules wrapped in a cylinder, as shown in Fig. 1 (*3*, *4*). These structures are unusual, because most organic membranes form either flat sheets or nearly spherical vesicles. Tubules have been observed in a number of systems of chiral organic molecules, including diacetylenic lipids (*3*, *5*), surfactants (*6*), bile (*7*), and glutamates (*8*). In diacetylenic lipid systems, they have a typical diameter of 0.5 μm and a typical length of 50 to 200 μm. They have been used for a variety of technological applications, including electroactive composites and controlled-release systems (*1*).

Several investigators have developed theories that explain the formation of tubules in terms of an intrinsic bending force in a chiral membrane (*7*, *9*–*13*). Although the details of these theories differ, they are all based on the same physical principle of chiral packing. The essential point is that long chiral molecules do not pack parallel to their nearest neighbors but rather at a non-zero twist angle with respect to their nearest neighbors. This favored twist angle can be visualized by packing hard screws together. In liquid crystals, the favored twist angle gives the pitch of a cholesteric phase. In systems of organic membranes, where the chiral molecules are confined to bilayers, the effects of the twist are more subtle. If the membrane is in a tilted phase, with the molecules tilted with respect to the local layer normal, the favored twist from neighbor to neighbor leads the whole membrane to twist into a cylinder, as illustrated in Fig. 2. The diameter of the cylinder can be calculated in terms of the favored twist and the molecular tilt.

So far, experiments on tubules have given only limited support to this theoretical model. Although there is strong evidence against competing theories (*1*, *13*), there has been only indirect evidence in favor of chiral molecular packing in tubules. This indirect evidence comes from the observation that most tubules exhibit a helical substructure or have helical microstructures as precursors to tubule formation. For example, diacetylenic lipid tubules formed in water and in ethanol-water systems commonly show helical patterns (Fig. 1A) (*14*–*16*). However, diacetylenic lipid tubules formed in methanol-water systems show no indication of

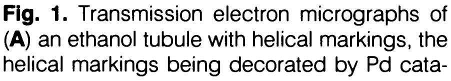

Fig. 1. Transmission electron micrographs of (**A**) an ethanol tubule with helical markings, the helical markings being decorated by Pd catalyst particles, compared to (**B**) a methanol tubule with no visible helical markings.

J. M. Schnur, B. R. Ratna, J. V. Selinger, A. Singh, Center for Bio/Molecular Science and Engineering, Naval Research Laboratory, Washington, DC 20375, USA.

G. Jyothi and K. R. K. Easwaran, Molecular Biophysics Unit, Indian Institute of Science, Bangalore 560012, India.

*To whom correspondence should be addressed.